Search for a K^-K^-pp double kaonic nucleus using the $d(K^-, K^0)$ reaction with the HypTPC detector

S. Hasegawa, S. Hayakawa, Y. Ichikawa (Spokesperson), K. Imai, H. Sako,

S. Sato, K. Tanida
Japan Atomic Energy Agency (JAEA), Japan

T. Nagae (Co-spokesperson)
Kyoto University, Japan

S. Ishimoto, S. Suzuki, T. Takahashi, M. Ukai
High Energy Accelerator Research Organization (KEK), Japan

K. Hicks
Ohio University, USA

J.K. Ahn, S.W. Choi, W.S. Jung, B.M. Kang, S.H. Kim, S.B. Yang
Korea University, Korea

S.H. Hwang
Korea Research Institute of Standards and Science, Korea

K. Joo
University of Connecticut, USA

Version 1.0, June 12, 2019

Short summary of the Proposed Experiment

Beamline:	K1.8
Beam:	2.0 GeV/c K^-
Beam intensity:	5×10^5 /spill (2×10^{11} in total)
Flat-top:	2 sec (5.52 sec/spill)
Target:	Liquid deuterium 5 cmϕ
Reaction:	$d(K^-, K^0)$
Spectrometer etc.:	Hyperon Spectrometer(HS), HypTPC
Beam time:	30 days + 1 day for hydrogen target run
	+1 day for empty target run + 3 days for setup
Estimated Yield:	6×10^3 events in total

Abstract

A simplest kaonic nucleus called as a K^-pp was searched using various reactions and positive results were shown by FINUDA and DISTO experiments. At J-PARC, E15 and E27 experiments were carried out to search for the K^-pp. Both J-PARC experiments reported the positive results recently. However, the obtained binding energy and decay width are not consistent each other and theoretical interpretation of these results is not conclusive. In order to confirm the kaonic nuclei and understand the detail property, the further experiment is essential. We propose to search for a K^-K^-pp (a four body state with isospin $I = 0$) by using $d(K^-, K^0)$ reactions at K1.8 beam line. The K^-K^-pp is chosen because the binding energy strongly depends on the $\bar{K}N$ interaction compared with the other kaonic nuclei. The K^- beam will be measured by K1.8 beam-line spectrometer and K^0 will be reconstructed by HypTPC detector. Moreover, we will also reconstruct the decay products of the K^-K^-pp as "K^-K^-pp" $\to \Lambda\Lambda$ or $\Lambda\Sigma^{\pm}\pi^{\mp}$ or Ξ^-p. The large acceptance of HypTPC is a key of this experiment.

1 Scientific Justification

Extensive studies of hypernuclei provide us a rich information such as YN and YY interaction and deformation of core nucleus. The extension of nucleus shows us the new possibility and property of hadrons. Here, a new concept of extended nuclei called as kaonic nuclei is predicted theoretically. The kaonic nuclei are quasi bound-state of $\bar{K}$ and nucleus. It is quite unique because meson exists as a real particle inside nucleus. Namely, there is a degree of freedom of anti-quark as constituent elements inside the nucleus. Then, whether or not kaonic nuclei exist is the one of the most important issue for the hadron physics.

The kaonic nuclei in medium-weight nucleus system were predicted by Kishomoto in 1999 [1]. Akaishi and Yamazaki discussed the possibility of deeply bound kaonic-nuclei in few body system in 2002 [2]. From this period, a study of the kaonic nuclei has been actively performed from both theoretical and experimental sides. Especially, the simplest kaonic nuclei called as the K^-pp, which is a quasi bound-state of a $\bar{K}$ and two nucleons with isospin $I = 0$ and spin parity $J^P = 1/2^-$, has been studied actively.

The first experimental result of the K^-pp was reported by the FINUDA collaboration [3]. They used the stopped K^- absorption reaction on ^{6,7}Li and ^{12}C targets and found a broad bump structure in the Λp invariant-mass spectrum. The DISTO collaboration also reported the possible signal of the K^-pp by using the $pp \to K^+\Lambda p$ reaction at $T_p = 2.85$ GeV [4]. The obtained binding energy of FINUDA and DISTO experiments corresponds to be about 100 MeV. The DISTO collaboration also

reported there was no signal at 2.5 GeV. The HADES collaboration measured the same $pp \to K^+\Lambda p$ reaction at 3.5 GeV, and found no signal [5]. No peak was observed in the inclusive spectrum of the $d(\gamma, K^+\pi^-)X$ reaction at $E_\gamma = 1.5 - 2.4$ GeV at LEPS [6].

At J-PARC, E15 and E27 experiments were carried out to search for the K^-pp at K1.8 BR and K1.8 beam-line, respectively. The E27 collaboration used $d(\pi^+, K^+)\Sigma^0 p$ reaction at $p_{\pi^+} = 1.69$ GeV/c and observed a broad bump structure [7]. The deduced binding energy and decay width were 95 $^{+18}_{-17}$ (stat.) $^{+30}_{-27}$ (syst.) MeV and 162 $^{+87}_{-45}$ (stat.) $^{+66}_{-78}$ (syst.) MeV, respectively. The E15 collaboration found the distinct peak-structure in the Λp invariant mass of ^{3}He$(K^-, \Lambda p)n$ reaction [8]. The binding energy and decay width of Breit-Wigner fit were evaluated as 47 $\pm$3 (stat.) $^{+3}_{-6}$ (syst.) MeV and 115 $\pm$7 (stat.) $^{+10}_{-20}$ (syst.) MeV, respectively. Moreover, the parameter of S-wave Gaussian reaction form-factor was also evaluated as $Q = 381 \pm 14$ (stat) $^{+57}_{-0}$ (syst.) MeV.

It is well known that the $\bar{K}N$ interaction has a strong attraction in the $I = 0$ channel. The strong attraction of this channel is a key to form the bound state of kaonic nuclei. The K^-pp has been also studied from the theoretical side using different treatments of the $\bar{K}N$ interaction and few-body calculation method [9].

For the $\bar{K}N$ interaction, we can categorize them into two types. One is energy dependent potentials and the other is energy-independent one. These two types show the different binding energy of the K^-pp and different interpretation of $\Lambda(1405)$. Here, $\Lambda(1405)$ is predicted as a first exited state of Λ baryon in the constituent quark-model. However, the observed mass of $\Lambda(1405)$ is smaller by about 80 MeV than the prediction of constituent quark-model. Therefore, $\Lambda(1405)$ is considered not three quark state but exotic state. In case of the energy-dependent potential, the $\Lambda(1405)$ is composed of two poles: one is located around 1420 MeV with a dominant coupling to $\bar{K}N$ and the other is at around 1380 MeV with a strong coupling to $\pi\Sigma$. Usually, the energy-dependent potential is constructed by using chiral SU(3)-based potential. On the other hand, the phenomenological potential, which is energy independent, assumes the $\Lambda(1405)$ as a simple quasi bound-state of $\bar{K}N$ channel. Note that the only one pole exits in physical energy sheet in case of the chiral-SU(3) potential with energy-independent treatment [10, 11], while there are two pole in energy-dependent one as described. The remained pole corresponds to be higher pole, $\bar{K}N$ pole, of energy-dependent potential and the pole energy is about 1405 MeV. The lower pole, $\pi\Sigma$ pole, is in unphysical energy sheet. It is important that this difference originated not from model setting but from the energy dependence, namely off-shell property of the $\bar{K}N$ interaction.

This difference of the $\bar{K}N$ pole-position directly affects the strength of the attraction and binding energy of kaonic nuclei. The $\bar{K}N$ pole around 1420 MeV (energy dependent) corresponds to be the $\bar{K}N$ binding energy of 15 MeV, which is about a half of 1405 MeV pole (energy independent). The energy-dependent chiral-SU(3) potential becomes less attractive in the sub-threshold region than the energy-independent one. Then, the binding energy of the K^-pp of energy-dependent calculation should be much smaller than energy-independent one.

In Fig. 1, the calculated binding energy and decay width of the K^-pp are summarized together with experimental values. The experimental values are shown by red squares with statistical (blue bar) and systematic (green bar) errors. The theoretical values using the energy dependent and independent potentials are shown by circles and triangles, respectively. There are also two types of the calculation methods: one is a variational method with effective single-channel potential and the other is a Faddeev coupled-channel method. This difference is also distinguished by different fill colors as white (Faddeev) and black (variational) in Fig. 1.

As shown in Fig 1, the difference originating from the calculation methods is a little. On the

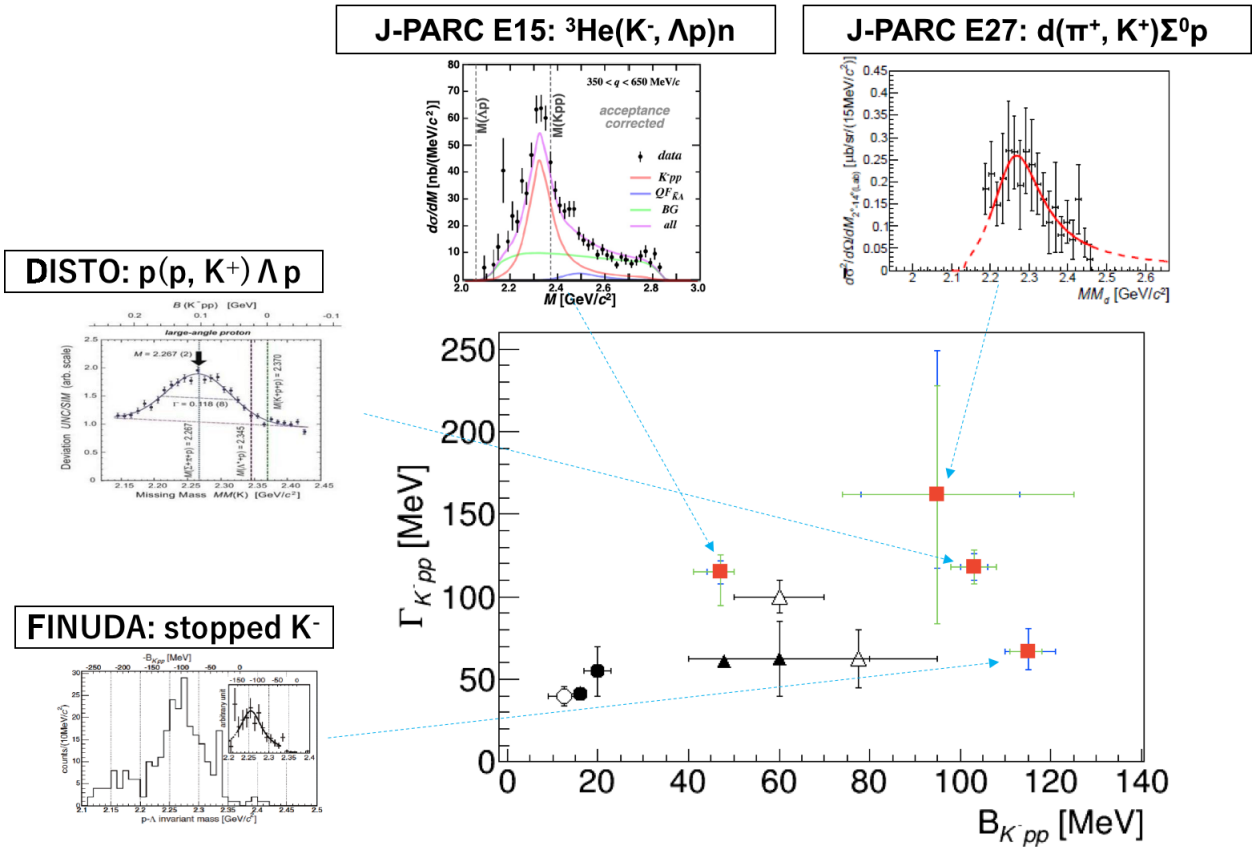

Figure 1: Summary of the calculated binding energy and width of the K^-pp listed in Ref. [9] together with the experimental values of the FINUDA [3], DISTO [4], J-PARC E15 [8], and E27 [7]. The theoretical values of energy dependent and independent potential are shown by circles and triangles, respectively. The difference of the calculation method is distinguished by different fill colors as white (Faddev) and black (variational). The experimental values are shown by red squares with the statistical (blue bars) and systematic (green bars) errors. See the text for the detail.

other hand, the binding energy strongly depends on the $\bar{K}N$ interaction as described. The binding energy of energy-dependent potential is smaller than the one of energy independent calculation. In Ref. [11], they discussed the difference of binding energy between energy dependent and independent potentials, both of which were derived by effective chiral Lagrangian. The calculated binding energies of energy dependent and independent potential were 9–16 and 44–58 MeV, respectively. This comparison is good indication to discuss the $\bar{K}N$ interaction by the K^-pp.

The experimental values are not consistent each other as shown in Fig. 1. Moreover, the experimental values are not consistent with theoretical one except for the E15's result with energy-independent calculation. The K^-pp binding energy of about 100 MeV, which was measured by FINUDA, DISTO, and E27 experiments, is not easy to reproduce theoretically. Here, there are some possible scenarios to interpret these results. One is a two pole possibility of the K^-pp [11, 12]. Namely, two baryon system also may have the two pole structure same as one baryon system as the $\Lambda(1405)$. In this case, higher and lower poles will be strongly coupled with $\bar{K}NN$ and $\pi\Sigma N$ channels, respectively. The lower pole-position corresponds to be the K^-pp binding energy of about 100 MeV. The results of FINUDA, DISTO, and E27 may be related to be this lower pole. Moreover, the another possibility of $\pi\Lambda N$–$\pi\Sigma N$ dibaryon [13] can be considered for the interpretation of the E27's result.

The E15's result is almost consistent with the calculation using the energy independent $\bar{K}N$ interaction. The data quality such as statistics and detector acceptance of this experiment was good. Moreover, the possibility that this resonance peak related to be the K^-pp is high because they used K^- induced reaction. However, the obtained Q-distribution, angular distribution of (K^-, n) reaction, is not easy to interpret this resonance as $J^P = 0^-$ state, ground state of the K^-pp. In the E15's reaction, it can be considered that the K^-pp will be produced via two-step three-body absorption as K^-+"n" $\to K^-+n$, K^-+"pp" $\to$"K^-pp" $\to \Lambda+p$, where "n" and "pp" are nucleons inside ^{3}He and "K^-pp" is the K^-pp bound state. Thus, the angular distribution of (K^-, n) of the K^-pp production should have a forward peak by comparing with the K^-+"n" $\to K^-+$"n" quasi-elastic reaction, if the spin parity of resonance state is $J^P = 0^-$. It is because that spin parity of ^{3}He is $J^P = 1/2^+$ and proton pair inside ^{3}He should be spin singlet. However, the obtained Q-dependence of resonance state had the backward peaking distribution compared with a one of a "QF"-like three-body absorption [8]. Then, the measured resonance peak of E15 may be related to be excited state. In this case, the ground state as $J^P = 0^-$ may corresponds to be the bump of FINUDA, DISTO, E27. Note that E15 collaboration evaluated parameter of reaction form factor by assuming that the K^-pp is produced from one-step three-body absorption. The interpretation of the E15's result depends on the reaction mechanism to produce the K^-pp.

Needless to say, the systematic study of kaonic nuclei is important in order to conclude the discussion of $\bar{K}N$ interaction and $\Lambda(1405)$ and to understand the detail property of kaonic nuclei. Moreover, it is also important to conclude the interpretation of the K^-pp. Here, we summarize the theoretical values of binding energy of various kaonic nuclei in Fig. 2. The values of Ohnishi-chiral1, 2, and Ohnishi-AY are taken from Ref. [14]. The Ohnishi-chiral1 and 2 were calculated by using energy-dependent chiral-SU(3) potential. The difference of chiral1 and 2 originates the different picture of kaonic nuclei. The chiral1 corresponds to be the picture in which $\bar{K}$ field collectively surrounds the remained nucleons and chiral2 corresponds to be the picture in which $\bar{K}$ energy is distributed equally. The Barnea-chiral in Fig 2 also used energy-dependent chiral SU(3) potential [15]. The difference between Ohnishi [14] and Barnea [15] is come from the treatment of complex value of $\bar{K}N$ two-body energy, E, in the many-body system. In case of Ohnishi's calculation, they adopted

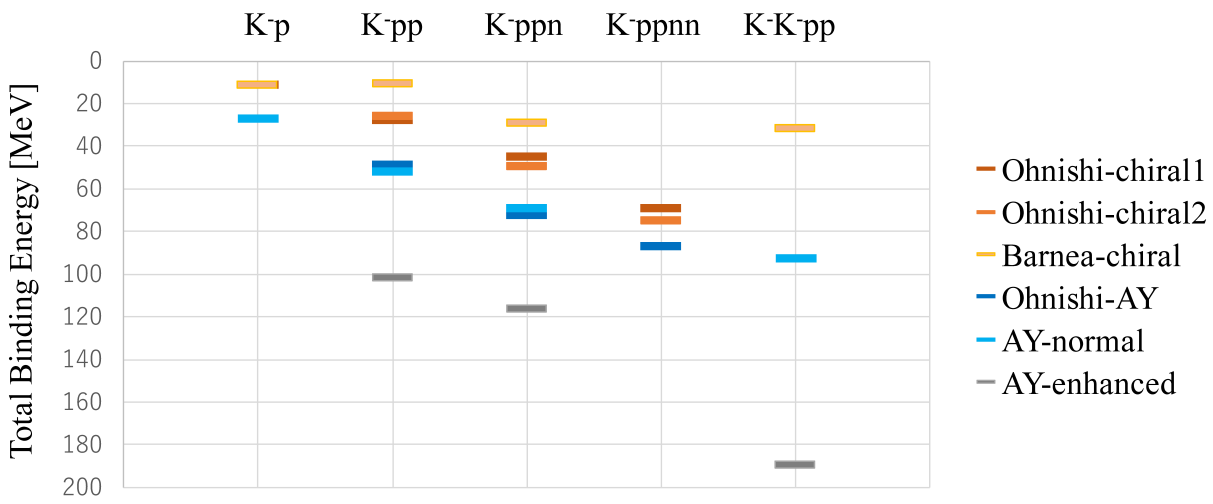

Figure 2: A dependence of the calculated binding-energy of kaonic nuculei. Ohinishi-chiral1, 2 [14], and Barnea-chiral [15], which are shown by warm colors, are calculated by using energy dependent potential based on the chiral SU(3). Ohnishi-AY [14] and AY-normal [16], which are shown by cold colors, are used the phenomenological energy-independent potential. The phenomenological one assumes the $\Lambda(1405)$ as pure $\bar{K}N$ state. AY-enhanced [16] used much stronger $\bar{K}N$ potential by enhancing attraction to reproduce very deep binding-energy of the K^-pp as FINUDA, DISTO and E27.

the $\bar{K}N$ interaction as $V_{\bar{K}N}(r, E)$ type, while Barnea's one was $V_{\bar{K}N}(r,\ \mathrm{Re}[E])$. The $\bar{K}N$ interaction of $V_{\bar{K}N}(r, E)$ becomes more attractive than the one of $V_{\bar{K}N}(r,\ \mathrm{Re}[E])$. However, the Ohnishi's K^-pp binding-energy seems to be still lower than the E15's one.

Ohnishi-AY [14] and AY-normal [16] used the phenomenological $\bar{K}N$ interaction by assuming the $\Lambda(1405)$ as pure $\bar{K}N$ quasi bound-state. This phenomenological potential is energy independent. The calculation methods of these results are different, while they are good agreement. Ohinishi-AY used stochastic variational method with correlated Gaussian basis and AY-normal adopted the Faddeev calculation. This potential seems to well reproduce the K^-pp binding-energy of the E15, about 50 MeV, as described. In Ref. [16], they also discussed the enhanced $\bar{K}N$ potential to reproduce the very deep binding-energy of the K^-pp, about 100 MeV, as the FINUDA, DISTO, and E27. They pointed out it is necessary to enhance the $\bar{K}N$ attraction by 25% to reproduce the deep K^-pp state as shown by a gray bar, AY-enhanced, in Fig. 2. Since the mass and width of $\Lambda(1405)$ which is related to be two body $\bar{K}N$ system can not be changed, they inferred the enhancement is due to in-medium effect in dense kaonic nuclei. Namely, this inference means that the shrinkage of kaonic nuclei due to strong attraction makes a high density and the $\bar{K}N$ attraction becomes much stronger due to a partial restoration of chiral symmetry.

In any case, the total binding-energy of kaonic nuclei will change as function of number of $\bar{K}$ and nucleon systematically, as shown in Fig. 2. Thus, we can conclude the discussion of $\bar{K}N$ interaction, $\Lambda(1405)$, and K^-pp by the systematic study of kaonic nuclei. Here, the double kaonic nucleus, K^-K^-pp, more strongly depends on the $\bar{K}N$ interaction. It means that the binding energy of K^-K^-pp is more sensitive for the $\bar{K}N$ interaction than the other single kaonic-nuclei.

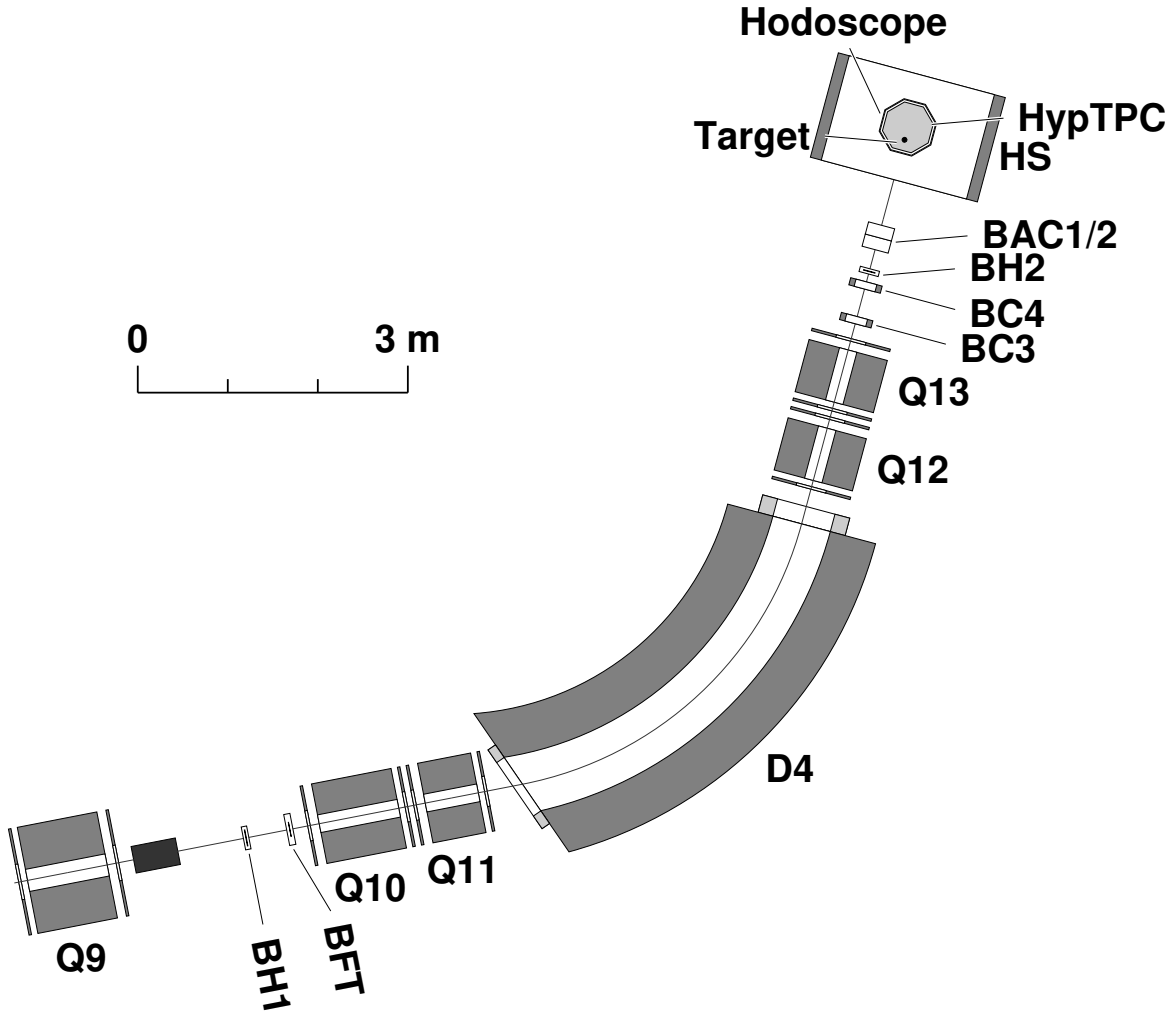

Figure 3: A schematic view of experimental setup at K1.8 beam-line of the J-PARC Hadron Hall.

It is because that the K^-K^-pp has two $\bar{K}N$ pairs and the probability of isospin $I_{\bar{K}N} = 0$ is large. Therefore, the K^-K^-pp is really important piece to understand the kaonic nuclei. Of course, to study the other kaonic nuclei such as K^-ppn and K^-ppnn is also important. The promising reaction to produce the single kaonic-nuclei is (K^-, N) as the E15. We hope that such experiments to search for the other single kaonic-nuclei will also be carried out and compare the result each other.

2 Experimental Method

The proposed experiment will be performed at the K1.8 beam-line together with the Hyperon Spectrometer (HS) developed for J-PARC E42, 45, and 72 experiments as shown in Fig. 3. The K^-K^-pp quasi-bound state is produced via $K^-d \rightarrow$"K^-K^-pp"K^0 reaction at 2.0 GeV/c. The K^- beam will be analyzed by using K1.8 beam-line spectrometer. K^0 and the decay product of K^-K^-pp as "K^-K^-pp" $\rightarrow \Lambda\Lambda$ or $\Lambda\Sigma^\pm\pi^\mp$ or Ξ^-p will be reconstructed by HypTPC. Here, K^0 will be identified by measuring $K^0_s \rightarrow \pi^+\pi^-$ decay. $\Lambda\Lambda$ mode will be identified by measuring $\Lambda \rightarrow p\pi^-$ decay. In case of $\Lambda\Sigma^\pm\pi^\mp$ mode, Λ will be reconstructed by using $\Lambda \rightarrow p\pi^-$ decay and $\Sigma^\pm$ will be identified by missing mass of $d(K^-, K^0\Lambda\pi^\mp)X$ reaction, where X should be $\Sigma^\pm$. Moreover, we can also measure the $\pi^\pm$ or proton from $\Sigma^\pm$ decay. The $\Lambda\Sigma^\pm\pi^\mp$ mode will be identified by combining

these information. $\Xi^- p$ final state will be reconstructed by measuring $\Xi^- \to \Lambda\pi^-, \Lambda \to p\pi^-$ continuous decay. Namely, 6 charged particles will be measured by HypTPC in any decay modes.

2.1 The K1.8 Beam-line Spectrometer

The secondary K^- beam, which will be produced at a primary T1 target by irradiating a primary proton beam, will be delivered to the K1.8 beam-line. The K1.8 beam-line is designed to provide separated secondary particles with the momentum up to 2 GeV/c by using double electrostatic separators (ESS1 and 2). The last part of K1.8 beam-line is the K1.8 beam-line spectrometer. The schematic view of K1.8 beam-line spectrometer is shown in Fig. 3. The K1.8 beam-line spectrometer consisted of timing plastic scintillation hodoscopes (BH1 and 2), a fiber tracker (BFT), $QQDQQ$ magnets (Q10, Q11, D4, Q12, and Q13), two sets of multi-wire drift chambers (BC3 and 4), and aerogel Čerenkov counters (BAC1 and 2).

BH1 and 2 are plastic scintillation-counters segmented into 11 modules and 5 modules, respectively. These hodoscopes will be used as a trigger and time-of-flight counters for beam particles with a typical time resolution of about 100 ps. The BH2 determines the time reference for all other detectors. BFT is 1-mm diameter scintillating fibers, the scintillating light of which was detected by Multi-Pixel Photon Counter (MPPC) devices, installed at the upstream part of the $QQDQQ$ system [17]. BFT measures the horizontal coordinate of the beam trajectories and has a sensitive are of $160^{\mathrm{H}} \times 80^{\mathrm{V}}$ mm^2. It is consisted of two layers stagged by 0.5 mm with a position resolution of about 0.2 mm in rms.

BC3 and 4 are multi-wire drift chambers with 1.5 mm drift spaces installed at the exit of the last Q magnet ($Q13$). They have six layers ($xx'uu'vv'$) configuration, where x plane measured the horizontal hit position. The u and v planes are tilted by $\pm$ 15° with respect to the x plane. The typical position resolution of BC3 and 4 is about 0.2 mm in rms. The momenta of beam particles are reconstructed from the track information of these detectors (BFT, BC3, and BC4) by using the third-order transfer matrix through the $QQDQQ$ system. The design value of the momentum resolution is 3.3×10^{-4} (FWHM) with the position accuracy of 0.2 mm (rms) [18].

BAC1 and 2 are threshold-type silica aerogel Čerenkov counters with a refractive index of $n = 1.03$, which corresponds to the threshold momentum of 0.6 GeV/c for $\pi^{\pm}$. These detectors are installed at the downstream of BH2. The K^- beam detection efficiency is about 95% including the inefficiency due to the decay in-flight between BH1 and BAC's. The pion detection efficiency for each BAC is evaluated to be more than 99%.

2.2 Hyperon Spectrometer (HS)

The Hyperon Spectrometer (HS) consists of a large-acceptance superconducting dipole magnet, a Time Projection Chamber (HypTPC) and a TPC hodoscope. The schematic view of HS setup is shown in Fig. 3. The detail design, expected performance, and the status of development of HS are described in the Techinical Design Report of E42/45 experiments [19, 20].

Figure. 4 shows the schematic view of the superconducting dipole magnet with liquid target system, which is developed for the E45 experiment. The superconducting Helmholtz-type dipole-magnet is chosen to meet the requirements for the Hyperon Spectrometer. The magnet symmetry-axis is perpendicular to the beam direction. The reached maximum magnetic-field strength is 1.29 T, which corresponds to be 85% of the design value of 1.5 T. The proposed experiment chooses the magnetic field as 1 T as same as E42 experiment.

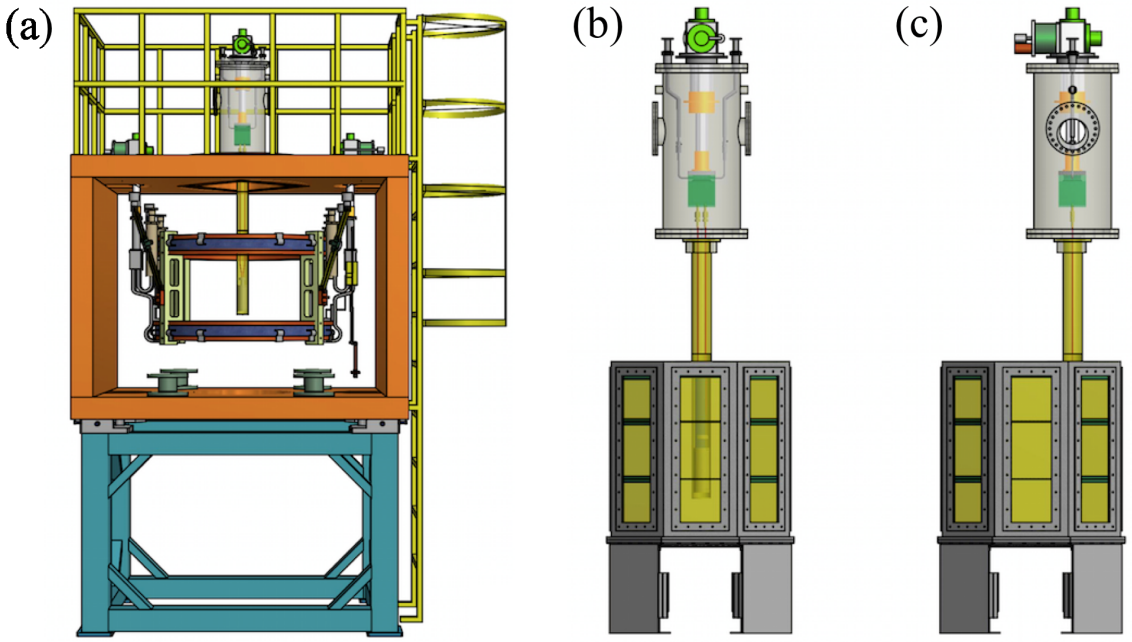

Figure 4: (a) Schematic view of superconducting magnet with liquid target system. (b) Front view of HypTPC with liquid target system. (c) Side view of (b).

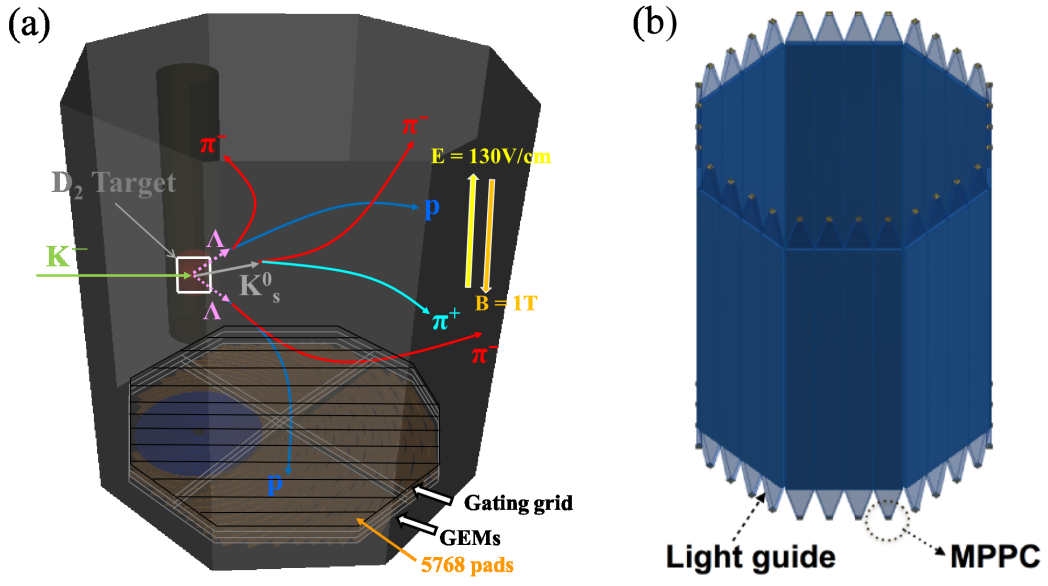

Figure 5: (a) A schematic drawing of HypTPC. (b) A schematic drawing of the TPC hodoscope.

The HypTPC is main detector of HS to measure the tracks of the charged particles and reconstruct the decay vertexes of hyperons such as Λ decays into $p\pi^-$ and $\Sigma^\pm$ decays into $N\pi$. In this proposed experiment, the K^0_s particles of the $K^- + d \rightarrow$"K^-K^-pp"K^0 reaction and the decay products of K^-K^-pp as "K^-K^-pp" $\rightarrow \Lambda\Lambda$ or $\Lambda\Sigma^\pm\pi^\mp$ or Ξ^-p will be reconstructed by the HypTPC as shown in Fig. 5 (a).

The liquid deuterium target will be installed inside the TPC volume to achieve the large acceptance. The detail information of the liquid target system is described in the Techinical Design Report of E45 experiment [20]. Figure 4 (b) and (c) shows the schematic view of the HypTPC with services for the liquid target hydrogen/deuterium target (front and side views, respectively). The target is positioned 143 mm upstream from the magnet and HypTPC center to achieve the large acceptance. The averaged momentum resolutions ($\Delta p/p$) for proton and π^- are estimated to be about 2.7 % and 1.4% in σ, respectively. Here, the structure of the target holder and the field cage were designed to ensure an uniform electric field to achieve a good momentum resolution.

In order to operate the TPC under the high particle-rate condition, we adopt the triple GEMs (Gas Electron Multiplier) amplification for the signal detection and the gating-wire grid to suppress the ion backflow. Moreover, the P-10 (Ar-CH_4 (90:10)) gas, whose maximum drift velocity is 5.3 cm/s, is selected for the high particle-rate capability. The higher drift velocity has advantage for the high rate operation to reduce the accidental track rate.

The GEM is more stable against discharge compared with wire chambers under the high particle rates. Furthermore, we adopt the triple GEM configuration with two 50 μm GEMs for the top and middle layers and a 100 μm GEM for the bottom layer, where 50 μm GEM and 100 μm GEM are the GEMs with 100 and 50 μm thickness, respectively. This order is chosen to minimize the ion backflow to the drift volume and achieve the higher gain at the lower discharge-rate condition. Each GEM sheet has segmented structure of electrodes in the upper face in order to reduce the spark rate.

The gating-wire grid is installed in order to suppress positive ions flowing into the drift volume. It is placed 4.2 mm above the top GEM layer. It is made of gold-plated Cu-Be wires of 50 μm in diameter and the adjacent wires are separated by 1 mm.

The signal, which is amplified by the triple GEMs, is read out by the concentric anode-pad plane. The readout-pad configuration has been optimized for spatial resolution to be 0.2–0.3 mm at the gas gain of 10^4. The inner sector has 10 radial pad rows with pads of 9 mm in length and 2.1–2.7 mm in width, and the outer sector has 22 pad rows with pads of 12.5 mm in length and 2.3–2.4 mm width, resulting in a total of 5768 pads.

The front end electronics based on GET (a Generic Electronic System for TPCs) [21] reads out the charge detected by the anode pad plane. The GET system can optimize the gain, shaping time, and FADC frequency. The pad signals are sent out to the inputs of AsAd (ASIC and ADC) boards through discharge projection-boards (ZAP). The AsAd board houses 4 AGET chip, each having 64 channels for signal amplification and shaping, 256 channels in total. The HypTPC signals are read out by 31 AsAd boards.

In order to test the basic performance and high rate capability of HypTPC, we commissioned the HypTPC using 230 MeV protons with beam rates up to 1 MHz at HIMAC. This test experiment was carried out without magnetic field. The spatial resolutions on the pad plane were measured to be 400–700 μm, which corresponds to be 250–300 μm in magnetic field of 1 T. Even at the 1 MHz beam rate, the triggered event was well separated from non-triggered events at earlier and later times by using a Hough transformation method. The measured pad-efficiency of about 98% was

almost not changed up to 1 MHz beam rate. Moreover, we observed no significant change in the transverse and longitudinal spatial resolutions under the high-rate condition. We concluded that the HypTPC achieved the sufficient performance to carry out the actual experiment at J-PARC. The detail results of the HIMAC test are described in the NIM paper of HypTPC [22].

The TPC hodoscope consists of a 32 segments of plastic scintillator and enclose the HypTPC as shown in Fig. 3 and 5 (b). The segment size is 80 cm long, 7 cm wide, and 1 cm thick. The TPC hodoscope is installed to provide the multiplicity trigger and measure the time of flight for the particle identification. The $\pi/K/p$ particles will be identified by combining the information of the time of flight, dE/dx of HypTPC, and momentum. Since it is difficult to use PMT due to strong magnetic field of 1 T, we will use MPPCs as a right sensor.

The 8 MPPCs are attached on each side of the scintillator to ensure the sufficient number of photons for the good time resolution. We developed the new circuit to readout 8 MPPC signals. Here, the series-connection method is widely used to achieve the good time resolution. However, this method requires the higher bias voltage ($\sim 60 \times n$ V, where n is number of MPPCs). It is not easy to prepare the power supply to output higher voltage with low electrical noise for 8 MPPCs connection. Moreover, the pulse height of series connection becomes $1/n$ because the overall capacitance should be C_0/n, where C_0 is capacitance of single MPPC. Thus, we developed the "mixer connection" method for the new circuit. In this method, the bias voltage is applied in parallel and the signal are summed after amplification by pre-amplifier. We adopt the AD8000 ultra-fast Op-amp [23] for both pre-amplifier and the sum logic. Then, we performed the bench test by using cosmic ray with actual size scintillator with the new circuit for 8 MMPCs readout. The measured time resolution was about 120 ps, which is sufficient to distinguish π^+ and proton [20].

3 Simulations

3.1 Trigger

The trigger will be determined by using the multiplicity of TPC hodoscope combining the kaon beam trigger defined as BH1 $\times$ BH2 $\times$ $\overline{(\mathrm{BAC1}||\mathrm{BAC2})}$. The multiplicity trigger of TPC hodoscope will be also used for E45 and 72 experiments.

In this proposed experiment, 6 charged particles will be emitted in any decay modes of the K^-K^-pp as described. For example, $\pi^+\pi^-$ pair from $K^0_s \to \pi^+\pi^-$ decay and 2 $p\pi^-$ pairs from "K^-K^-pp" $\to \Lambda\Lambda \to p\pi^-p\pi^-$ decay will be detected by HypTPC. Figure. 6 (a) shows a multiplicity distribution of the TPC hodoscope of this decay mode simulated by using GEANT4 code. The black line shows the raw multiplicity distribution and the red one is additionally required the track reconstruction by HypTPC. As shown in Fig. 6 (a), there are the multiplicity > 6 events, while 6 charged particles as $\pi^+\pi^-$ from K^0_s and 2 $p\pi^-$ pairs from 2Λ are emitted in this simulation. It is because, sometimes, one charged particle makes multiplicity = 2 when particle injects horizontal edge of scintillator. The hodoscope scintillator has a thickness of 1 cm and each segment is not overlapped. The mean of multiplicity is about 5 because the coverage of TPC hodoscope is not 100%, while it has sufficiently large acceptance.

Since we will use the multiplicity of TPC hodoscope in the trigger level, the total acceptance is determined by TPC hodoscope, while we can reconstruct the tracks and perform the particle identification by using the information of momentum and dE/dx of HyTPC without the TPC hodoscope. The acceptance as a function of required multiplicity is shown in Fig. 6 (b). We can

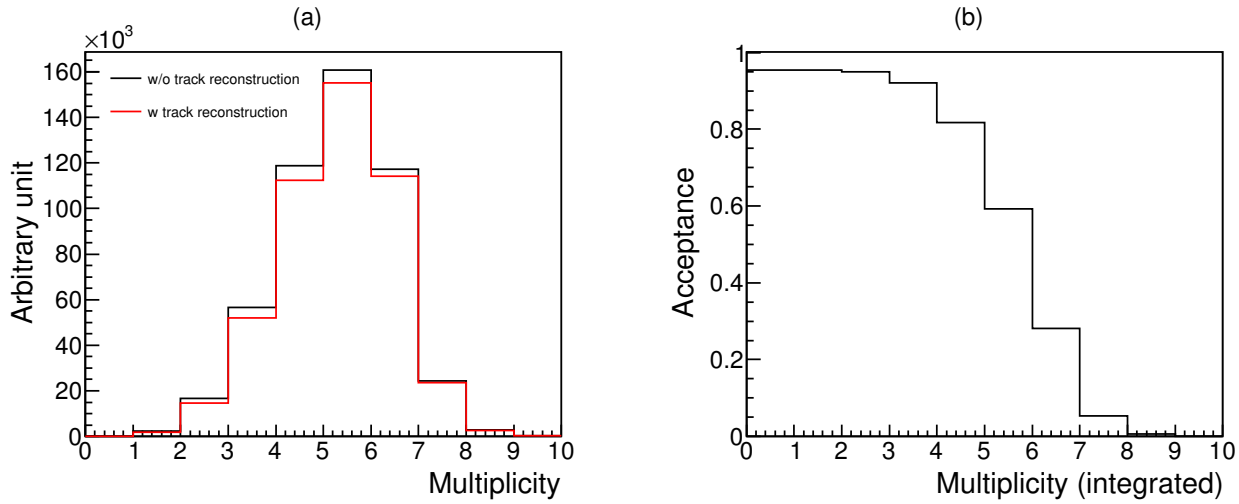

Figure 6: (a) Simulated multiplicity distribution of TPC hodoscope for the K^-K^-pp signal. (b) The acceptance distribution of K^-K^-pp as function of multiplicity of TPC hodoscope. $K^-K^-pp \to \Lambda\Lambda$ mode is chosen both in (a) and (b) histograms.

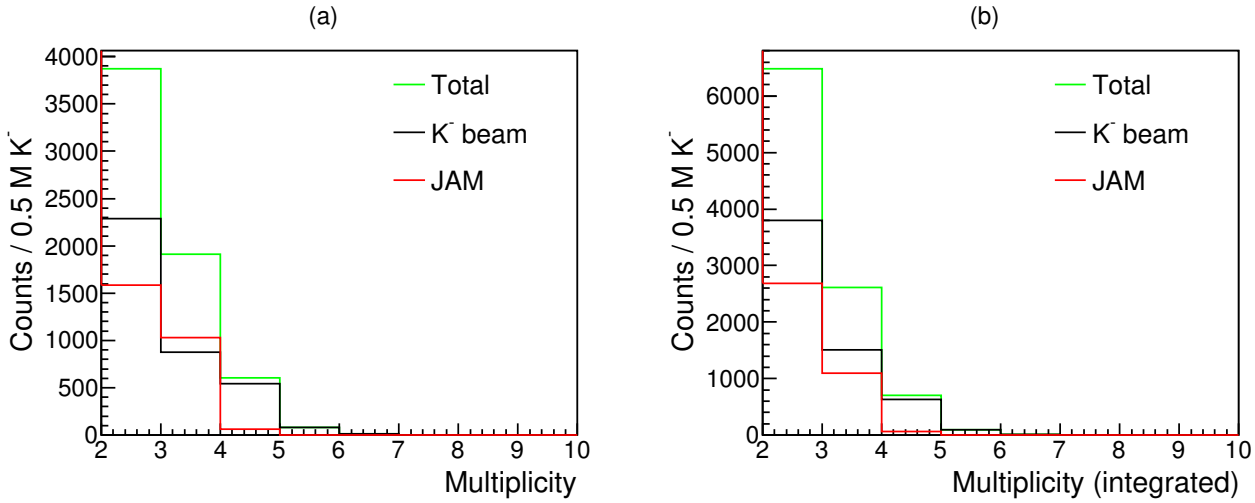

Figure 7: The simulated multiplicity distributions for background processes. The black and red lines are component of decay in flight of K^- beam and possible K^-d reactions estimated by JAM code, respectively. The total distributions are shown by black lines. The vertical axises of (a) and (b) are raw and integrated multiplicity distributions, respectively. The horizontal axises are normalized by 0.5 M K^- beam, $\sim$1 spill.

keep the large acceptance more than 80% when we require the multiplicity ≥ 4 in the trigger level.

On the other hand, the multiplicity distributions of the background processes are important to determine the trigger condition. We simulated the multiplicity distributions of the decay in flight

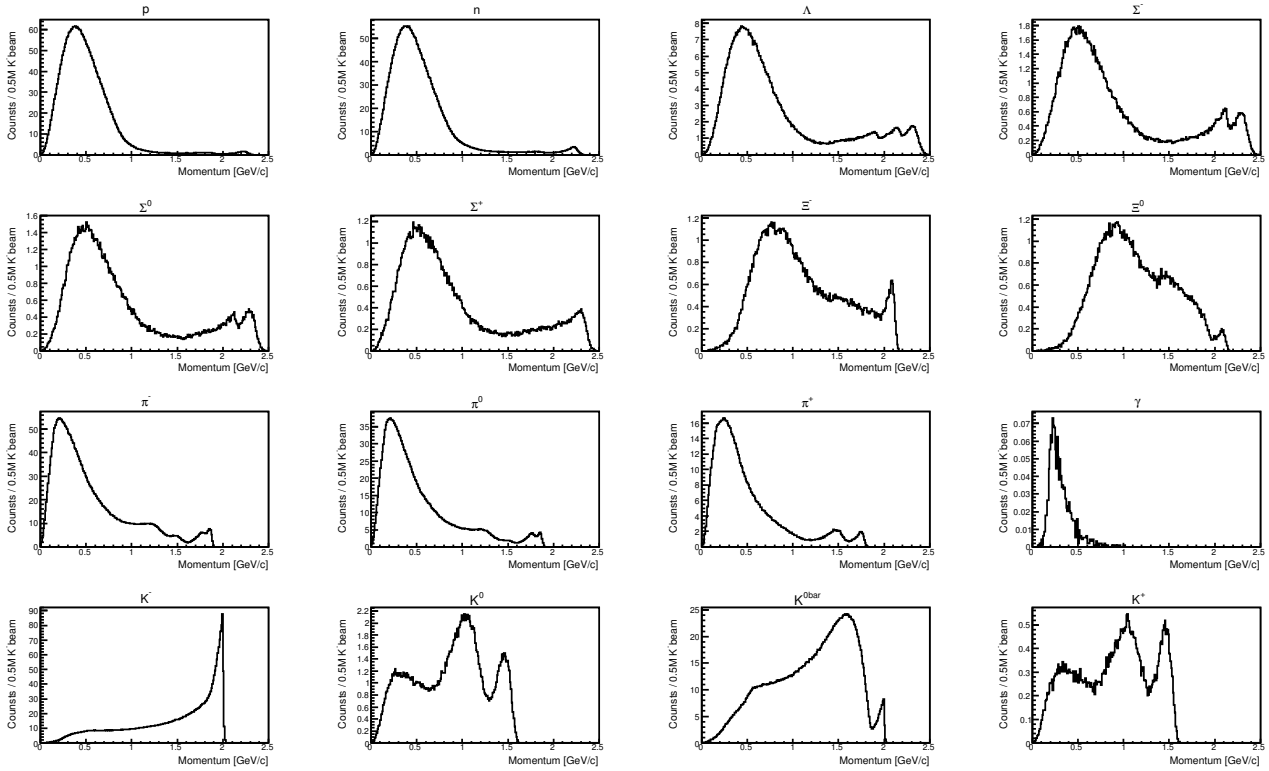

Figure 8: The simulated momentum distribution of each particle emitted by K^-d reaction at 2.0 GeV/c. These distributions are estimated by using JAM code. The horizontal axis is normalized by 0.5 M K^- beam, $\sim$1 spill.

of the K^- beam and possible K^-d reactions by using JAM code [24]. The estimated distributions are shown in Fig. 7. The detail results using JAM code is described in Sec. 3.2. The black and red lines are one of the component of decay in flight of K^- beam and the K^-d reaction (JAM), respectively. The total distributions are shown by green lines. The vertical axises of (a) and (b) are raw and integrated multiplicity distributions, respectively. The horizontal axises are normalized by 0.5 M K^- beam, corresponding to be $\sim$1 spill. As shown in Fig. 7 (b), the estimated trigger-rate in condition of multiplicity ≥ 3 and 4 are about 2600 and 700 counts / spill, respectively. These values corresponds to be the DAQ efficiency of 85% and 96%, respectively, when we select the DAQ option as a number of time bins of 256 [20]. The estimated trigger-rate is lower than E45 because E45 will require the multiplicity = 2 as the trigger. The actual trigger condition will be determined by checking the actual trigger rate and considering the figure of merit. Note that the estimated trigger rate is sufficiently suppressed and the acceptance is enough to carry out this experiment.

3.2 Expected Result

In this proposed experiment, we will use $d(K^-, K^0_s)$ reaction at 2.0 GeV/c. Here, it is well known that there are huge backgrounds such as a charge exchange reaction of $d(K^-, \bar{K^0}_s)$. We will suppress this $\bar{K^0}$ background by requiring the hyperon production additionally. On the other hand, the

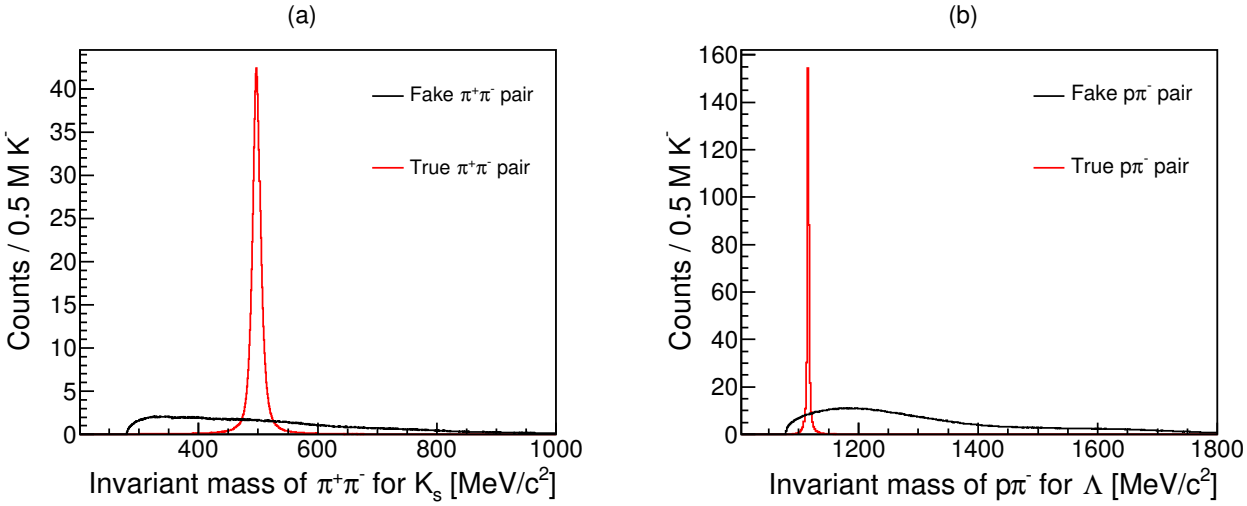

Figure 9: (a) Simulated invariant mass distribution of $\pi^+\pi^-$ pair. (b) Simulated invariant mass distribution of $p\pi^-$ pair. Red line shows the distribution by selecting true $\pi^+\pi^-$ and $p\pi^-$ pairs from K_s and Λ decays, respectively. Black lines are chosen the fake $\pi^+\pi^-$ and $p\pi^-$ pairs.

physical background such as a non-resonant two-body absorption reaction of $K^-d \to K^0\Lambda\Lambda$ should also exist. Therefore, we simulate the possible background processes of K^-d reactions at 2.0 GeV/c by using JAM code [24]. In JAM code, hadrons and their excited states are explicitly propagated in space-time by cascade method.

Figure. 8 shows the simulated momentum-distribution of each particle emitted by $K^-d \to X$ reaction at 2.0 GeV/c. The horizontal axis is normalized by 0.5 M K^- beam, $\sim$1 spill, where 1 bin corresponds to be 10 MeV/c. We estimate the background component by inputting the JAM output to the GEANT4 simulation of HypTPC. As shown in Fig. 8, we input momentum vectors of proton, neutron, Λ, Σ, Ξ, π, γ, and K, where the decay of resonance particles such as $\Delta^{(*)}$, N^*, Y^*, and K^* are taken into account inside JAM code.

In Fig. 9, we demonstrate the selection quality of K_s and Λ by invariant mass of $\pi^+\pi^-$ and $p\pi^-$ pairs, respectively. Red lines show the true $\pi^+\pi^-$ and $p\pi^-$ pairs from K_s and Λ decays, respectively. Black lines are chosen the fake $\pi^+\pi^-$ and $p\pi^-$ pairs. These distributions are also estimated by GEANT4 simulation combing with JAM. Here, the momentum resolution for the reconstruction of invariant mass is included by assuming the position resolution of HypTPC as described in Sec. 2.2. As shown in Fig. 9, the HypTPC has a sufficient resolution to select the K_s and Λ from the continues backgrounds.

As described, it is well known that there are huge backgrounds such as a charge exchange reaction of $d(K^-, \bar{K^0}_s)$. We need to suppress these backgrounds to search for the K^-K^-pp because the cross section of K^-K^-pp production is expected to be small. In Fig. 10, we demonstrate how to suppress the backgrounds. Black line of Fig. 10 (a) shows the simulated missing-mass distribution of inclusive $d(K^-, K_s)$ reaction. Red and Green lines of this figure are selected K^0 and $\bar{K^0}$ as K_s, respectively. As you can see, there is also large contribution of $d(K^-, K^0)$ reaction and we need to suppress it for the K^-K^-pp search, while $d(K^-, \bar{K^0})$ is dominant reaction. Then, we additionally require Λ detection as shown in blue and magenta lines, where $\Lambda \geq 1$ and $\Lambda = 2$ is

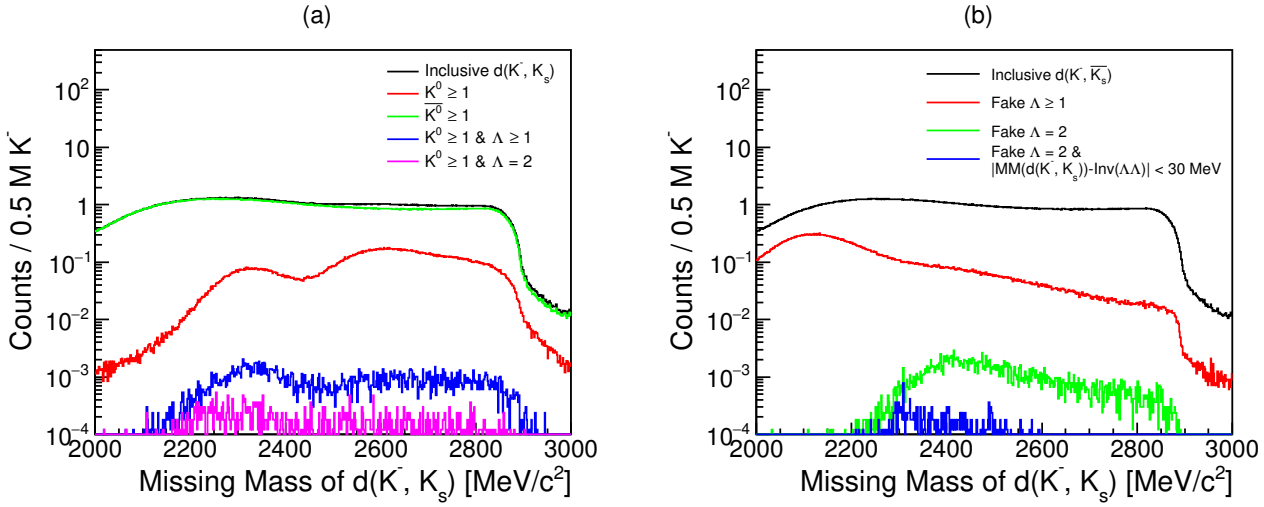

Figure 10: Simulated missing-mass distribution of background $d(K^-, K_s)$ reaction. (a) Black line is the distribution of inclusive $d(K^-, K_s)$ reaction. Red and Green lines are selected K^0 and $\bar{K^0}$ as K_s, respectively. The $\Lambda \geq 1$ and $\Lambda = 2$ are additionally required in blue and magenta lines, respectively. (b) Black line is the distribution of inclusive $d(K^-, \bar{K^0})$ reaction. In red and green lines, the (p, π^-) pair production, in which invariant mass is near Λ mass, is addition required. In blue line, the consistency between missing mass of $d(K^-, K_s)$ and invariant mass of $\Lambda\Lambda$ is additionally required.

required, respectively. We can suppress the $d(K^-, K^0)$ background in order of 10^{-2} by requiring $\Lambda\Lambda$ detections additionally because the dominant component of this background is quasi-free reactions.

The $d(K^-, \bar{K^0})$ reaction can be drastically suppressed by requiring Λ detection because Λ should not be produced in this reaction. The suppression is demonstrated in Fig. 10 (b). The inclusive missing-mass distribution of $d(K^-, \bar{K^0})$ reaction is shown by black line. The Λ can not be produced in this reaction, but $p\pi^-$ pair can be produced and the invariant mass of $p\pi^-$ pair can be inside the Λ selection region. We call this $p\pi^-$ pair as fake Λ and the selected region is defined as $|M(p\pi^-) -$ PDG Λ mass $| < 30$ MeV/c^2. In red and green lines, we additionally require the number of fake Λ as fake $\Lambda \geq 1$ and fake $\Lambda = 2$, respectively. Moreover, we also require the consistency between missing mass of $d(K^-, K_s)$ and invariant mass of $\Lambda\Lambda$ as shown in blue line. By requiring these selections, we can suppress the backgrounds of both $d(K^-, K^0)$ and $d(K^-, \bar{K^0})$ reactions.

Finally, we compare the signal of K^-K^-pp and the possible background for $d(K^-, K^0)\Lambda\Lambda$ reaction as shown in Fig. 11. Red line shows the signal distribution of K^-K^-pp of $K^-d \to$"K^-K^-pp"K^0, "K^-K^-pp" $\to \Lambda\Lambda$ reaction. The cross section of this reaction is assumed as 1 μb, which is same assumption for H-dibaryon in the E42 experiment. Here, the cross section of K^-pp of the kaon induced reaction measured by the E15 experiment is $\sigma^{tot}_{K^-pp} \cdot Br_{K^-pp\to\Lambda p} = 11.8$ μb. Thus, our assumed cross section of the K^-K^-pp is about 1/10 of one the K^-pp. The mass and width of the K^-K^-pp are assumed as 2810 MeV and 100 MeV corresponding to be $2\Lambda(1405)$. By assuming 30 days beam time, the estimated yield is about 6×10^3 events.

Green line shows the background distribution of non resonant two-body absorption reaction as $K^-d \to K^0\Lambda\Lambda$ estimated by using JAM code. Since this reaction is physical background, it is difficult to suppress, while there is small contribution around the K^-K^-pp signal region. Moreover,

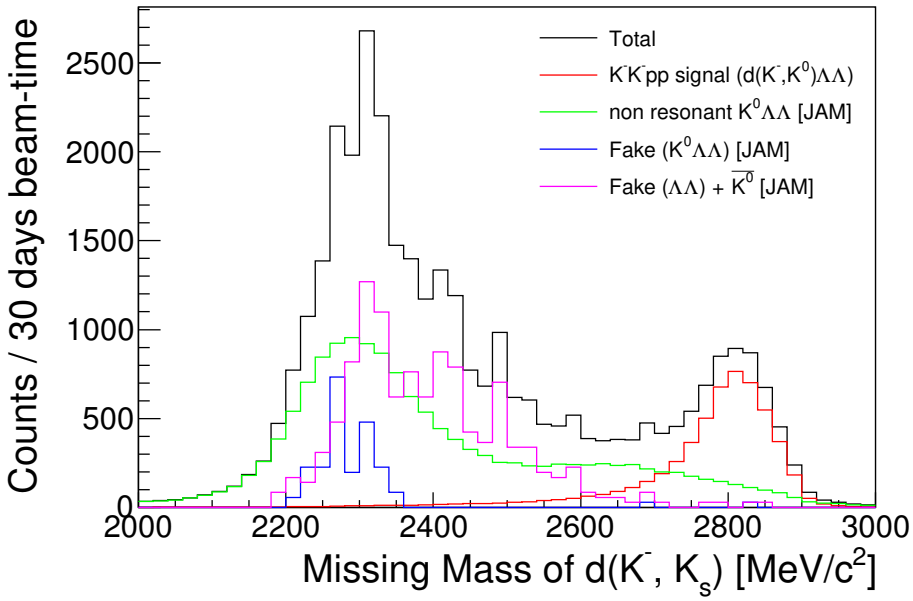

Figure 11: Comparison between the K^-K^-pp signal and possible background component of $d(K^-, K^0)\Lambda\Lambda$ reaction. See the detail in text.

we will select the scattered angle to find the good signal / background region to enhance the K^-K^-pp signal. Blue and magenta lines are the distribution of fake $K^0\Lambda\Lambda$ combinations. In case of blue line, the fake K^0 and fake 2Λ are chosen. The magenta line is required true $\bar{K^0}$ and fake 2Λ pairs. Here, the definition of fake K^0 is $|M(\pi^+\pi^-) - \text{PDG } K_s \text{ mass}| < 50$ MeV/c^2, by considering invariant-mass resolution of K_s as shown in Fig. 9. Moreover, the consistency between missing mass of $d(K^-, K_s)$ and invariant mass of $\Lambda\Lambda$ is required. Note that the fake $K^0\Lambda\Lambda$ components can be estimated and subtracted by checking the side region of selected region of K_s and Λ.

Finally, we confirm that the background contributions are not so large around the K^-K^-pp signal region and it is possible to search for the K^-K^-pp by this method. Moreover, we can also search for a H-dibaryon at the same time in this experiment because quantum number of the K^-K^-pp is same as the H-dibaryon. We can also measure the final state of $\Lambda\Sigma^\pm\pi^\mp$ and Ξ^-p. We may be possible to discuss the size of "K^-K^-pp" by comparing the branching ratio with theoretical calculation. Intuitively, the size is expected to be small if Ξ^-p branch is large.

4 Run Plan and Beam Time Request

We request 30 days for the main beam time, based on yield estimation described in the previous section. In addition, we need following beam times.

- 3 days for detector and target commissioning.
- 1 day for hydrogen target run.

- 1 day for empty target run.

The hydrogen target data will be taken to check the performance of HypTPC by measuring $p(K^-, K^0)\Xi^0$ reaction as the calibration. The momentum correction will be carried out by checking the invariant mass of K^0 and Λ emitted from Ξ^0 decay and missing mass for the Ξ^0 production. Moreover, the evaluated cross-section of Ξ^0 production will be compared with past experiments. It is important to discuss the systematic error of the efficiency and effective thickness of experimental target. The differential cross section, angular distribution, will also be compared with past data to evaluate the ambiguity of acceptance correction. The empty target data will be taken to estimate the possible background originating from the target cell.

We will be able to start the proposed experiment by the end of FY2020, when the commissioning of HypTPC is finished. However, the proposed experiment shares HS with E42, E45, and E72 experiments. We cannot start within two months of beam times of E42 and E72 experiments. It is because the target system such as target holder is different from E42, where E42 will use diamond as a target. E72 will be done at K1.8 BR beam-line and we need to move HS to K1.8 beam-line if the proposed experiment will be performed after E72. Since the experimental setup of the proposed experiment is almost same as E45, we do not need time to exchange detectors. Finally, it may be possible to perform the proposed experiment by sharing the K1.8 experimental area with S-2S spectrometer system because HS is compact as shown in Fig. 3.

5 Summary

We propose to search for the double kaonic nucleus K^-K^-pp by using the $d(K^-, K^0)$ reaction at 2.0 GeV/c. Within 30 days of physics data taking, we can acquire about 6×10^3 events of the K^-K^-pp production signal. The proposed experiment is important to confirm the kaonic nuclei and understand the detail property of them. We can also search for the H-dibayon at the same time because the quantum number of the K^-K^-pp is same as the H-dibayon. The large acceptance and good momentum resolution of HypTPC is a key to succeed the proposed experiment.

References

[1] T. Kishimoto, Phys. Rev. Lett. **83**, 4701 (1999).

[2] Y. Akaishi and T. Yamazaki, Phys. Rev. C **65**, 044005 (2002).

[3] M. Agnello *et al.*, Phys. Rev. Lett. **94**, 212303 (2005).

[4] T. Yamazaki *et al.*, Phys. Rev. Lett. 104, 132502 (2010).

[5] G. Agakishiev *et al.*, Phys. Lett. B **742**, 242 (2015).

[6] A. O. Tokiyasu et al., Phys. Lett. B **728**, 616 (2014).

[7] Y. Ichikawa *et al.*, Prog. Theor. Exp. Phys. **2015**, 021D01 (2015).

[8] S. Ajimura *et al.*, Phys. Lett. B **789**, 620 (2019).

[9] A. Gal, Nucl. Phys. A **914**, 270 (2013).

[10] Y. Ikeda, and T. Sato, Phys. Rev. C **76**, 035203 (2007).
Y. Ikeda, and T. Sato, Phys. Rev. C **79**, 035201 (2009).

[11] Y. Ikeda, H. Kumano and T. Sato, Prog. Theor. Phys. **124**, 533 (2008).

[12] A. Doté, T. Inoue, and T. Myo, Prog. Theor. Exp. Phys. **2015**, 043D02 (2015).

[13] H. Garcilazo and A. Gal, Nucl. Phys. A **897**, 167 (2013).

[14] S. Ohnishi *et al.*, Phys. Rev. C **95**, 065202 (2017).

[15] N. Barnea, A. Gal, E.Z. Liverts, Phys. Lett. B **712**, 132 (2012).

[16] S. Maeda, Y. Akaishi and T. Yamazaki, Proc. Jpn. B **89**, 418 (2013).

[17] R. Honda *et al.*, Nucl. Insrum. Meth. A **787**, 157 (2015).

[18] T. Takahashi *et al.*, Prog. Theor. Exp. Phys. 2012, 02B010 (2012).

[19] Technical Design Report of J-PARC E42 experiment.

[20] Technical Design Report of J-PARC E45 experiment.

[21] E. Pollacco *et al.*, Nucl. Instrum. Meth. A **887** 81, (2018).

[22] S.H. Kim *et al.*, submitted to Nucl. Instrum. Meth. A.

[23] https://www.analog.com/media/en/technical-documentation/data-sheets/ad8000.pdf

[24] Y. Nara: A Microscopic Transport Code for high energy nuclear collisions,
http://quark.phy.bnl.gov/~ynara/jam/;
Y. Nara *et al.*, Phys. Rev.C **61**, 024901 (2000).